The Astrophysical Journal, 796:29 (14pp), 2014 November 20 doi:10.1088/0004-637X/796/1/29

MODELING MHD ACCRETION–EJECTION: EPISODIC EJECTIONS OF JETS TRIGGERED BY A MEAN-FIELD DISK DYNAMO

Deniss Stepanovs, Christian Fendt, and Somayeh Sheikhnezami
Max Planck Institute for Astronomy, Königstuhl 17, D-69117 Heidelberg, Germany; deniss@stepanovs.org, fendt@mpia.de
Received 2014 July 25; accepted 2014 September 23; published 2014 October 31

ABSTRACT

We present MHD simulations exploring the launching, acceleration, and collimation of jets and disk winds. The evolution of the disk structure is consistently taken into account. Extending our earlier studies, we now consider the self-generation of the magnetic field by an $\alpha^2\Omega$ mean-field dynamo. The disk magnetization remains on a rather low level, which helps to evolve the simulations for $T > 10{,}000$ dynamical time steps on a domain extending 1500 inner disk radii. We find the magnetic field of the inner disk to be similar to the commonly found open field structure, favoring magneto-centrifugal launching. The outer disk field is highly inclined and predominantly radial. Here, differential rotation induces a strong toroidal component, which plays a key role in outflow launching. These outflows from the outer disk are slower, denser, and less collimated. If the dynamo action is not quenched, magnetic flux is continuously generated, diffuses outward through the disk, and fills the entire disk. We have invented a toy model triggering a time-dependent mean-field dynamo. The duty cycles of this dynamo lead to episodic ejections on similar timescales. When the dynamo is suppressed as the magnetization falls below a critical value, the generation of the outflows and also accretion is inhibited. The general result is that we can steer episodic ejection and *large-scale jet knots* by a *disk-intrinsic dynamo* that is time-dependent and regenerates the jet-launching magnetic field.

Key words: accretion, accretion disks – galaxies: jets – ISM: jets and outflows – magnetohydrodynamics (MHD) – stars: mass-loss – stars: pre-main sequence

Online-only material: color figures

1. INTRODUCTION

Astrophysical jets as highly collimated beams of high-velocity material and outflows with a small degree of collimation and lower speed are a ubiquitous phenomena in astrophysical sources of rather different ranges in energy output and physical extension. Previous calculations have shown that jets and winds could be produced by the interplay of large-scale magnetic fields with the accretion disk (Blandford & Payne 1982; Pelletier & Pudritz 1992; Ferreira 1997).

Two main mechanisms compete in the acceleration of the material that is lifted from the disk into the outflow. In addition to the classical magneto-centrifugal acceleration mechanism proposed by Blandford & Payne (1982), which is usually compared to a sling-shot mechanism of material along poloidally dominated magnetic field lines, acceleration may also be driven by a pressure gradient of the toroidal magnetic field, comparable to a mechanical spring mechanism. This mechanism has been studied extensively both analytically (Lynden-Bell & Boily 1994; Lovelace et al. 1995; Lynden-Bell 1996) and numerically (Ustyugova et al. 1995). If the toroidal magnetic field is generated continuously, inflation of the poloidal field structure results and the material enclosed by the poloidal magnetic loops is accelerated in the vertical direction. This kind of jet structure is known as a *tower jet*, or a Poynting-dominated jet.

The jet launching and collimation problem[1] is usually addressed numerically by applying a large-scale initial poloidal magnetic field. This holds in particular for simulations considering the acceleration and collimation processes only and assuming the underlying disk as a boundary condition (Ustyugova et al. 1995; Ouyed & Pudritz 1997; Krasnopolsky et al. 1999; Fendt & Čemeljić 2002; Fendt 2006, 2009; Pudritz et al. 2006; Vaidya et al. 2009; Porth & Fendt 2010).

Also, simulations treating the launching mechanism, i.e., simulations of the accretion–ejection structure that include the time evolution of the disk dynamics, have so far assumed a global large-scale magnetic field as an initial condition (Shibata & Uchida 1985; Casse & Keppens 2002, 2004; Meliani et al. 2006; Zanni et al. 2007; Tzeferacos et al. 2009; Murphy et al. 2010; Sheikhnezami et al. 2012; Fendt & Sheikhnezami 2013).

These studies have provided deep insight into the launching mechanism, i.e., the connection between the outflow and the underlying disk. It is clear today that the magnetic field plays a crucial role in lifting the matter out of the disk and accelerating it to high velocity. By knowing the disk magnetization, one can infer many details of the launched outflow, namely, its energetics and the ejection efficiency (see Zanni et al. 2007; Sheikhnezami et al. 2012; Stepanovs & Fendt 2014, hereafter Paper I).

It is still an open issue what the exact structure and the strength of the magnetic field in the disk are, and where its origin is. Besides a central stellar magnetic field or advection of magnetic field from the ambient medium, a turbulent dynamo can be a major source of the disk magnetic field (Pudritz 1981a, 1981b; Brandenburg et al. 1995). In studying the disk dynamo in the context of outflow launching, only a few numerical experiments have been performed in which the magnetic field was generated ab initio (Bardou et al. 2001; von Rekowski et al. 2003; von Rekowski & Brandenburg 2004). These authors were first to show how accretion disks start producing the outflow if the

[1] In this paper we apply the following notation. Jet *launching* is the process that lifts accreting material out of the disk and couples it to a disk wind (accretion–ejection structure). Jet *formation* is what we call the acceleration and collimation of that slow disk wind from the disk surface to a high velocity of super-escape speed, super-Alfénic speed, and possibly super-magnetosonic speed

magnetic field is amplified by the dynamo to about its equipartition value.

A further motivation for considering a disk dynamo for jet launching is seemingly the time-dependent ejection of the jet material. For protostellar jets the typical timescales for ejection derived from the observed knot separation and jet velocity are in the range of 10–100 yr. The typical timescale of the jet-launching area is, however, about 10–20 days, which is the Keplerian period close to the inner disk radius. A time-variable dynamo may be responsible for changing the jet-launching conditions on longer timescales. We may refer here to the dynamo cycle of the solar magnetic field, which is longer than the Sun's rotation period.[2]

Our main concern in this paper is the structure and time evolution of the dynamo-generated magnetic field, the launching of outflows by such a disk self-generated magnetic field, and the interrelation between the dynamo and the episodic ejection of jets, possibly leading to the co-called jet knots. Such a study has not yet been presented in the literature.

Disk dynamos were discussed in the literature on episodic accretion and ejection events in dwarf novae, and also as a possible physical process to generate MHD instabilities and turbulence, allowing for angular momentum transfer and accretion. Armitage et al. (1996) discussed a disk dynamo mechanism in accretion disks as a cause for dwarf novae eruption, similar to what could probably happen in jet-launching disks. Tout & Pringle (1992) discuss a disk dynamo action in order to physically produce the magnetic disk viscosity. However, Gammie & Menou (1998) showed that for low Reynolds numbers the MHD disk turbulence and angular momentum transport dies out, possibly leading to episodic accretion in dwarf novae.

Rozyczka et al. (1995) discuss a model of a disk dynamo driven by magnetic buoyancy, which does not directly involve a disk turbulence. This model was re-visited by Johansen & Levin (2008), who find that accretion could in fact be established by a Parker-instability-driven dynamo. According to Johansen & Levin (2008) accretion could be based on the interaction of Parker and magnetorotational instabilities (MRI). In this scenario the vertical component of the magnetic field is generated by Parker instability and serves as a source for MRI.

Applying a mean-field $\alpha^2\Omega$ dynamo (Krause & Rädler 1980) we present the step-by-step evolution of the magnetic field. In our approach turbulence is being addressed in the mean field approach, and is not self-consistently generated (e.g., by the MRI).

We also study episodic jet-launching scenarios by means of a simple toy model in which we artificially switch the dynamo action on/off. We discuss whether similar processes in which the dynamo does change its strength may lead to episodic jet ejection and the jet knots. We also discuss in detail how the magnetic field can be regenerated by re-establishing the dynamo action.

Our paper is organized as follows. In Section 2, we briefly describe our numerical setup. For a more complete discussion we refer to Paper I. In particular, we discuss the implementation of the mean-field dynamo equations and the model approach for the magnetic diffusivity and the dynamo-α. In Section 3, we present our reference dynamo simulation where the jet-launching magnetic field structure is dynamo-generated from a weak seed field. We discuss the difference between dynamo and non-dynamo simulations. In Section 4, we present simulations during which the disk dynamo is switched on and off repeatedly, leading to episodic ejection of the disk material into the collimated outflow. We summarize our paper in Section 5.

[2] By coincidence, the difference in the respective timescales—a magnetic cycle of 22 yr and a rotational period of 35 days—is comparable to those of protostellar jets.

2. MODEL APPROACH

For our numerical simulations, we apply the MHD code PLUTO[3] (Mignone et al. 2007), solving the time-dependent, resistive MHD equations on a spherical grid. Our simulations have been performed in two-dimensional axisymmetry, applying spherical coordinates (R, θ). We refer to (r, z) as cylindrical coordinates.

We have specified the equations considered in detail in Paper I. Here we stress in particular the induction equation that we have modified in the code according to the mean-field dynamo formalism (Krause & Rädler 1980),

$$\frac{\partial \boldsymbol{B}}{\partial t} = \nabla \times (\boldsymbol{V} \times \boldsymbol{B} + \overline{\overline{\alpha}}_{\rm dyn} \boldsymbol{B} - \overline{\overline{\eta}} \boldsymbol{J}), \quad (1)$$

where the tensor $\overline{\overline{\alpha}}_{\rm dyn}$ describes the α-effect of the mean-field dynamo, and the tensor $\overline{\overline{\eta}}$ the magnetic diffusivity (see below).

As no physical scales are introduced in the equations we solve, the results of simulations are presented in non-dimensional units. Lengths are given in units of R_0, corresponding to the inner disk radius. Velocities are given in units of $V_{\rm K,0}$, corresponding to the Keplerian speed at R_0. Thus, times are given in $T_0 \equiv R_0/V_{\rm K,0}$ units. Note that $\boldsymbol{2\pi T_0}$ corresponds to one rotation at the innermost orbit. Densities are given in units of ρ_0, corresponding to R_0. Pressure is measured in $P_0 = \epsilon^2 \rho_0 V_0^2$, where ϵ is the ratio of the initial isothermal sound speed to Keplerian speed taken at the disk midplane. All our simulations were performed with $\epsilon = 0.1$.

We normalize all variables, namely, R, ρ, V, and B, to their values at the inner disk radius R_0. We thus may apply our scale-free simulations to a variety of jet sources. For the typical astrophysical scaling of the code units we refer to Table 1 of Paper I.

We apply a numerical grid with equidistant spacing in the θ-direction, but stretched cell sizes in the radial direction, considering $\Delta R = R\Delta\theta$. Our computational domain of size $R = [1, 1500R_0]$, $\theta = [0, \pi/2]$ is discretized with $(N_R \times N_\theta)$ grid cells. We use a general resolution of $N_\theta = 128$. In order to cover a factor 1500 in radius, we apply $N_R = 600$. This gives a resolution of 16 cells per disk height (2ϵ) in the general case. We have also performed a resolution study with 1.5 times higher (lower) resolution, thus using 900×192 (450×64) cells for the domain, or 26 (11) cells per disk height.

2.1. Initial Conditions

As a measure for the magnetic field strength, we use the magnetization defined as the ratio between magnetic and thermal pressure,

$$\mu = \frac{B^2}{2P}. \quad (2)$$

We have used different prescriptions for the magnetization; however, in all cases the local magnetic field pressure $B^2/2$ is related to the gas pressure P at the midplane.

[3] Version 4.0, released 2013.

Table 1
Inner and Outer Boundary Conditions

	ρ	P	V_R	V_θ	V_ϕ	B_R	B_θ	B_ϕ
Inner disk	$\sim r^{-3/2}$	$\sim r^{-5/2}$	$\sim r^{-1/2}, \leqslant 0$	0	$\sim r^{-1/2}$	Slope	Slope	$\sim r^{-1}$
Inner corona	$\sim r^{-3/2}$	$\sim r^{-5/2}$	$0.2\cos(\varphi)$	$0.2\sin(\varphi)$	$\sim r^{-1/2}$	0	div B =0	0
Outer disk	$\sim r^{-3/2}$	$\sim r^{-5/2}$	Outflow, $\leqslant 0$	Outflow	Outflow	div B = 0	Outflow	$\sim r^{-1}$
Outer corona	$\sim r^{-3/2}$	$\sim r^{-5/2}$	Outflow, $\geqslant 0$	Outflow	Outflow	div B =0	Outflow	$\sim r^{-1}$
Axis	Sym	Sym	Sym	Anti-sym	Anti-sym	Sym	Anti-sym	Anti-sym
Equator	Sym	Sym	Sym	Anti-sym	Sym	Anti-sym	Sym	Anti-sym

Notes. Outflow is the zero gradient condition and the constant slope conditions are marked by "slope" in the table. Symmetric and anti-symmetric boundary conditions are marked by Sym and Anti-sym, respectively.

All dynamo simulations we perform start from a very weak initial magnetization $\mu_{\rm init} = 10^{-5}$. Therefore, the initial structure of the accretion disk can be obtained as the solution to the steady-state force equilibrium equation, neglecting the contribution by the Lorentz force,

$$\nabla P + \rho \nabla \Phi_{\rm g} - \frac{1}{R}\rho V_\phi^2 (e_R \sin\theta + e_\theta \cos\theta) = 0. \quad (3)$$

Assuming a self-similar disk structure this equation can be solved analytically.

All our simulations are initialized with a purely radial magnetic field, confined within the disk and defined via the vector potential $\boldsymbol{B} = \nabla \times A\boldsymbol{e}_\phi$, and

$$A = B_{\rm p,0} r^{-1} e^{-8z/H^2}. \quad (4)$$

The parameter $B_{\rm p,0} = \epsilon\sqrt{2\mu_{\rm init}}$ denotes the strength of the initial magnetic field, while $\epsilon = 0.1$ is the ratio of isothermal sound[4] to Keplerian speed. Although this magnetic field distribution may be considered as somewhat artificial, we found that it provides a smooth evolution during the initial phase. We have also performed simulations starting from a purely toroidal magnetic field as the initial condition, leading to very similar results.

In contrast, a purely vertical magnetic field would generate strong currents at the disk surface region because of the strong initial shear between the rotating disk and the non-rotating corona. This would greatly impact the initial evolution of the accretion–ejection structure. As long as the *initial* magnetization $\mu_{\rm init}$ is low, it does not play a substantial role in the initial disk evolution. This is the result of the exponential evolution of the magnetic field amplification by the dynamo.

2.2. Boundary Conditions

The boundary conditions are adapted from Paper I. The only change made was for the coronal region of the inner boundary. Here, we do not allow any magnetic flux to penetrate the inner coronal region and not only set $B_\phi = 0$, but also $B_R = 0$. Since the magnetic field vanishes in that area, we therefore prescribe a purely radial profile of the inflow into the corona (in contrast to an inflow aligned to the magnetic field considered previously), keeping the same inflow velocity $V_R = 0.2$. We summarize all boundary conditions in Table 1.

Since the magnetic field is suppressed in the inner coronal region, the shear in the area between the coronal region and the disk boundary can develop strong electric currents. This makes the region between the axis and the jet subject to small-scale perturbations, especially in the runs with high resolution. On the other hand, the jet-launching area of the inner disk always shows a smooth, stable, and non-fluctuating evolution.

[4] Note, however, that we use the adiabatic equation of state.

2.3. Magnetic Diffusivity

In Paper I, we studied in detail models with both a *standard diffusivity* and a so-called *strong diffusivity*. We have shown numerically that the standard diffusivity model is prone to the accretion instability. In the present paper, studying the dynamo action, we also performed simulations using both models. These models qualitatively share many similar features. Therefore, we will present simulations applying the strong diffusivity model, but commenting on differences between diffusivity models.

The main mediator in the magnetic diffusivity models is the magnetization of the underlying disk. In case of simulations with a substantially strong initial magnetic field (see Paper I), the disk magnetization is set by the magnetic field at the disk midplane.

Since in the dynamo simulations presented here the initial magnetic field does not intersect with the midplane,[5] and may also remain low for quite some time, the parameterization of the diffusivity model with the magnetization had to be revised. We keep the same notation as in Paper I for the strong diffusivity model,

$$\alpha_{\rm ssm} = \alpha_{\rm m}\sqrt{2\mu_0}\left(\frac{\mu_{\rm D}}{\mu_0}\right)^2, \quad (5)$$

where the *disk magnetization*,

$$\mu_{\rm D} = \frac{\langle B_{\rm D}\rangle^2}{2P}, \quad (6)$$

is defined by means of the *average* total magnetic field $\langle B_{\rm D}\rangle$ for a certain radius within the disk (up to H), normalized to the midplane pressure. A non-zero magnetic diffusivity allows for reconnection and diffusion of the magnetic field across the midplane. An assumption that the magnetic diffusivity is dependent on the total magnetic field strength is consistent with the fact that the MRI is excited by both toroidal and poloidal magnetic field components (Fromang 2013).

2.4. The Dynamo Model

We apply a standard mean-field $\alpha^2\Omega$ dynamo formalism (Krause & Rädler 1980), where α represents the dynamo effect by turbulence and Ω stands for the differential rotation of the plasma. According to the mean-field dynamo theory, an extra electromotive force term $\overline{\overline{\alpha}}_{\rm dyn}\boldsymbol{B}$ enters the induction equation (Equation (1)) and is responsible for the generation of the magnetic field. In general, $\overline{\overline{\alpha}}_{\rm dyn}$ is a tensor; however, non-diagonal components are less relevant for the dynamo process (Brandenburg & Donner 1997; Bardou et al. 2001),

[5] The initial field is purely radial or toroidal.

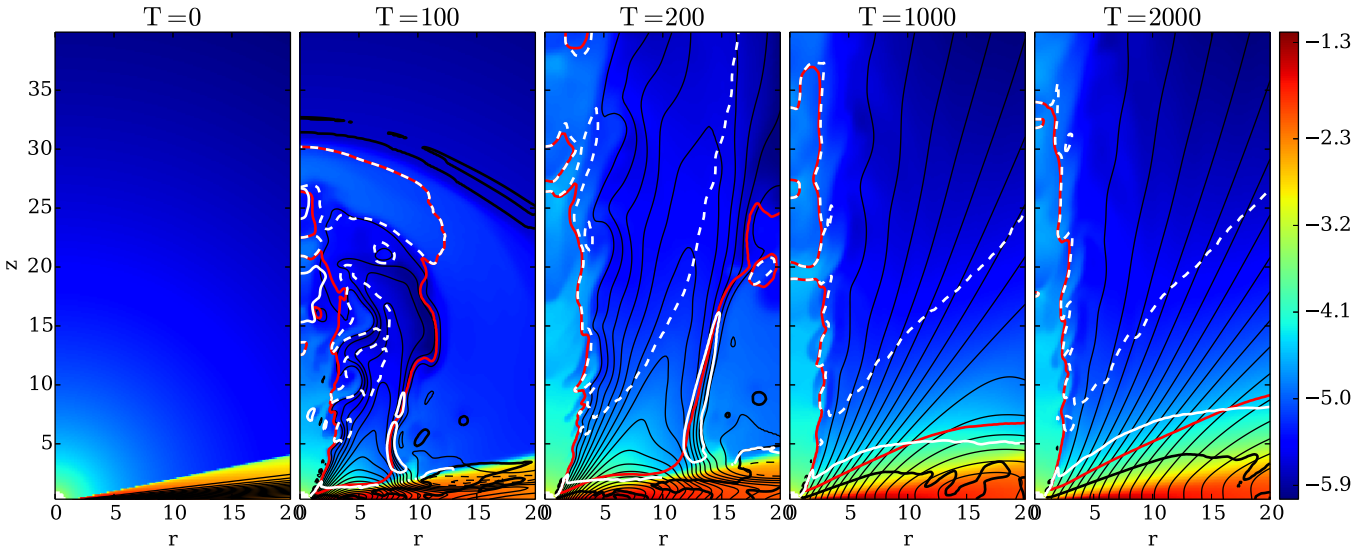

Figure 1. Time evolution of the disk–jet structure of the reference dynamo simulation. Only a small cylindrical part of the whole spherical domain is presented. Shown is the density (colors, in logarithmic scale); the poloidal magnetic field lines (thin black lines); the disk surface as defined by $V_R = 0$ (thick black line); and the sonic (red line), the Alfvén (white line), and the fast magnetosonic (white dashed line) surfaces.

(A color version of this figure is available in the online journal.)

in particular when a moderately strong magnetic field is present (Brandenburg et al. 2012). Therefore, we neglect all non-diagonal components and set the diagonal values equal to one parameter, $\alpha_{\rm dyn}$. The sign of $\alpha_{\rm dyn}$ as well as its number value in real disks has been widely debated (Brandenburg & Campbell 1997; Rekowski et al. 2000; Arlt & Rüdiger 2001). It has been shown that in order to get a dipolar structure of the mean magnetic field (as opposed to a quadrupolar structure), a negative alpha should be chosen (Brandenburg & von Rekowski 2007; Bardou et al. 2001).

Following a dimensional analysis, we may scale $\alpha_{\rm dyn}$ as the Keplerian velocity, thus applying

$$\alpha_{\rm dyn} = \alpha_{\rm D}\, r^{-1/2} F_\alpha(z), \tag{7}$$

where the vertical profile of α-effect is defined by

$$F_\alpha(z) = \begin{cases} \sin\left(\pi \dfrac{z}{H}\right) & z \leqslant H \\ 0 & z > H. \end{cases}$$

Here, H denotes the disk scale height and is approximated to be constant in time. The profile $F_\alpha(z)$ restricts the α-effect to the disk area.

It is generally believed that in the case of a strong magnetic field, the dynamo is quenched (Brandenburg & Subramanian 2005). The main reason is that a strong global magnetic field suppresses the turbulence, and thus the turbulent dynamo. The quenching is commonly applied by multiplying the $\alpha_{\rm dyn}$-term by a quenching function,

$$Q = \frac{1}{1 + 2\mu_{\rm x}}, \tag{8}$$

where $\mu_{\rm x}$, in contrast to $\mu_{\rm D}$, is the *local* magnetization. In order to be consistent with and directly affect the resulting magnetic field, we parameterize $\mu_{\rm x} = q_\mu \mu_{\rm D}$. By setting different q_μ we can limit the magnetic field growth to a certain value. Typically, we choose a rather high q_μ in order to quench the dynamo already for low magnetizations.

However, there is another possibility of limiting the magnetic field strength. We find that μ_0 in the strong diffusivity model (Equation (5)) is in fact a good measure for the resulting actual disk magnetization. This comes from the functional form of the diffusivity profile—any further growth of the disk magnetization has a strong feedback of the diffusivity (see Paper I).

Both direct dynamo quenching and indirectly limiting the magnetization by applying the strong diffusivity model lead to the saturation of the magnetic field. The difference between these approaches is that in the case of leaving the dynamo working in the disk, the magnetic flux is continuously generated and the disk is filled with the magnetic field. If the standard diffusivity model is applied, then dynamo quenching is the only mechanism to stop further magnetic field amplification. Therefore, since we apply the strong diffusivity model in the simulations we present, these simulations are run without dynamo quenching.

The expected dynamo number for accretion disks is given by

$$|D| = |C_\alpha C_\omega| \lesssim \frac{3}{2} {\alpha_{\rm ssm}}^{-2} \tag{9}$$

(von Rekowski et al. 2003), where $C_\alpha = (\alpha_0 H/\eta_0)$ and $C_\omega = (|\Delta\Omega| H^2/\eta_0)$ represent the strength of the α-effect and shear $d\Omega/dr$, respectively. Since our main concern is the resulting jet-launching magnetic field, we choose the maximum dynamo number in order to generate the magnetic field structure as rapidly as possible. The maximum dynamo number is provided by $\alpha_{\rm D} = -0.1$. Note that the dynamo number D is strongly dependent on $\alpha_{\rm ssm}$.

3. A REFERENCE DYNAMO SIMULATION

In this section, we discuss simulations applying the dynamo model and the resulting configuration of the disk–jet system.

We will refer to our reference dynamo simulation as the simulation with the parameters $\alpha_{\rm D} = -0.1$, $\alpha_{\rm m} = 1.65$, and $\mu_0 = 0.01$. Figure 1 shows the time evolution of our reference dynamo simulation, which can be seen as typical for our model setup. The simulation starts from a weak ($\mu_{\rm seed} = 10^{-5}$),

purely radial magnetic field, confined within the disk. Once the simulation is started, the toroidal component of the magnetic field is being continuously generated from the radial magnetic field simply by stretching. For the poloidal magnetic field component, the only generation mechanism is the dynamo effect that induces the poloidal component from the toroidal one.

Since the toroidal magnetic field is antisymmetric to the equator, the poloidal magnetic field loops that are generated by the dynamo first do *not* cross the equator. When they evolve over time, magnetic reconnection is enforced by the equatorial plane boundary condition and the magnetic diffusivity in the disk. As a consequence the magnetic loops (in the upper and lower hemisphere) merge and do traverse the equatorial plane. Since our diffusivity model depends on the average magnetic field in the disk there is always a substantial diffusivity present in the disk.

As described by Johansen & Levin (2008), the toroidal component of the magnetic field is continuously amplified until it reaches the buoyancy limit and starts moving upward, away from the disk. The upward motion changes the structure of the magnetic field lines from a predominantly radial one into a vertical direction. When the magnetic field is sufficiently inclined, magneto-centrifugal launching (Blandford & Payne 1982) can strongly accelerate the plasma on these field lines. The outflowing gas carries with it the toroidal magnetic field generated in the disk, thus setting a limit for the toroidal magnetic field strength in the disk (see Paper I).

All dynamo simulations evolve into three distinct domains in the accretion–ejection structure. Starting from the innermost disk, in the first region the magnetic field has the typical structure of field lines inclined with respect to the disk surface. Although magnetic field generation by the dynamo can still take place (if the α-effect is not quenched), the magnetization in that region has become sufficiently high in order to operate the standard magneto-centrifugal jet driving. The second region is where the poloidal magnetic field is mostly radial. Here the velocity shear in the disk creates a strong toroidal component of the magnetic field. In this area, the outflow is launched mainly by the buoyancy of the toroidal magnetic field.

The third region is the outer disk, where the magnetic field is rather weak, with somewhat irregular structure. Here, the magnetic flux has originated from the same magnetic loops as the innermost field, but because of the longer distance from the inner disk, the magnetic field strength has become much lower. Note that the magnetic field in the outer disk has the opposite polarity.

In summary, the overall structure of the magnetic field has a strong gradient that leads to strong outward diffusion of magnetic flux. Due to this diffusion, the whole disk is filled by a non-zero net magnetic field ($B_{\rm P}|_{\rm midplane} \neq 0$).

3.1. Dynamo Effect versus Magnetic Diffusion

As discussed in detail in Paper I, the evolution of the disk–jet system is mainly set by two opposite processes, the diffusion and advection of the magnetic field. It is more complicated to reach this balance. In the case of dynamo simulations, a third process contributes to the induction equation, the dynamo, and it is more complex to reach an equilibrium situation. Nevertheless, the main effects of these processes can be disentangled. The dynamo term in the induction equation manifests itself by generating loops of the poloidal magnetic field. Because of magnetic flux conservation along the magnetic loops, the magnetization in the inner disk (inner footpoint of the loop) is always higher than in the outer disk (outer footpoint of the loop). Therefore, a strong gradient in the magnetic field develops, which evolves primarily following the magnetic diffusivity model.

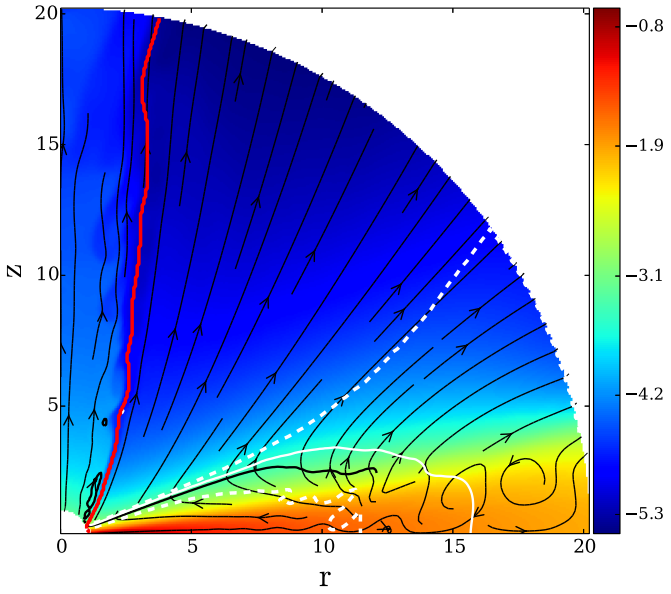

Figure 2. Snapshot at $T = 1000$ of physically different regions of the disk–jet structure. Shown is the mass density (in logarithmic scale) and stream lines of the poloidal velocity (black lines with arrows). The red line marks the magnetic field line that is rooted at the innermost disk area along the midplane. The upper white dashed line separates the area where $V_p || B_p$ from the rest of the disk. The accretion and ejection areas are separated by a white line indicating $V_r = 0$ and a black line indicating $F_\phi = 0$. The lower white dashed line separates the actual accretion area where $V_r \gg V_\theta$ from the rest of the disk.

(A color version of this figure is available in the online journal.)

By smoothing out the gradient of the magnetic field, the diffusivity plays a key role in the overall evolution of the magnetic field—first, it diffuses the magnetic field outward, thus filling the outer disk with the magnetic flux, and second, at the same time, the diffusivity destroys some flux within the magnetic loop by reconnection.

In general, if the dynamo is not sufficiently strong (in case of low dynamo numbers), the generated magnetic field will quickly decay (being diffused) and the magnetization necessary for jet-launching will not be reached.

3.2. Structure of the Tower Jet

Figure 2 shows the snapshot of the initial evolution at $T = 1000$.

What can be immediately seen is that the disk structure, namely, the structure of the velocity field and the magnetic field (see Figure 1), is completely different from the non-dynamo simulations (Stepanovs & Fendt 2014a, 2014b). We find two distinct regions in which the poloidal component of the magnetic field is inclined slightly (for $r < 10$) or strongly (for $r > 10$) with respect to the disk surface. While the magnetic field of the inner disk favors a standard magneto-centrifugal launching, in this section, we concentrate mainly on the outer disk.

In this region, the strong toroidal magnetic field is induced by the differential rotation of both the inclined poloidal magnetic field and by the magnetic loops that are rooted at radially different footpoints along the disk. The mechanism we observe is similar to the well-known tower jet (Lynden-Bell & Boily 1994; Lovelace et al. 1995; Lynden-Bell 1996; Ustyugova et al. 1995). The increasing toroidal magnetic field pressure leads to

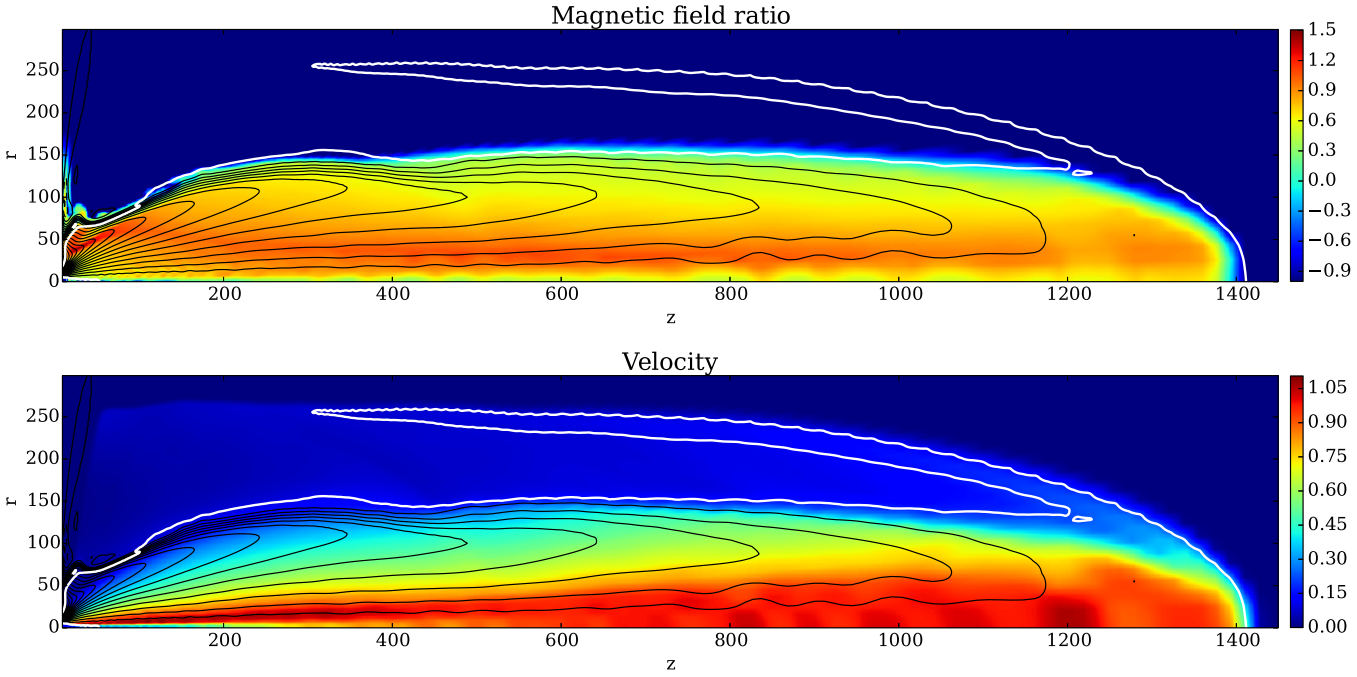

Figure 3. Structure of the simulation at $T = 1800$. Shown by the color: logarithm of toroidal to poloidal magnetic field ratio (upper plot) and the jet poloidal speed (lower plot). The black lines show the magnetic field. The white line represents the sonic surface.

(A color version of this figure is available in the online journal.)

an inflation of the poloidal magnetic loops and the material enclosed by that poloidal loops is accelerated in the vertical direction. This structure—typical for a tower jet—is clearly seen in the extended loops in Figure 3. In Figure 3, we further see that the fast jet, the one that is launched from the inner region of the disk, becomes collimated already close to the disk. On the contrary, for the tower jet—the expanding loop structures—it takes a while to collimate.

Almost everywhere in the jet region, the toroidal magnetic field dominates the poloidal magnetic field. Numerical simulations have shown that such structures, for example, naturally result from the interaction between a stellar dipole magnetic field penetrating the accretion disk (Hayashi et al. 1996; Ustyugova et al. 2000; Fendt & Elstner 1999, 2000; Kato et al. 2004). Note, however, that the magnetic loops presented in the disk are generated by the disk dynamo. The tower jet originates from the magnetic loop structure, and as the simulation evolves, that magnetic loop structure, and thus the base of the "tower," constantly moves outward.

Around the magnetic loop structure ($r \approx 10$), we find that it is the buoyancy force of the toroidal magnetic field that is the main force responsible for the lifting of the disk material into the outflow. Starting from the disk surface, defined as a surface of zero radial velocity ($V_R = 0$), the matter is further accelerated by the pressure gradient of the toroidal magnetic field. The latter is, in fact, consistent with the simulations by Ustyugova et al. (1995). The early evolution of the disk–jet system (Figures 3 and 1 at $T = 200$) clearly shows the similarity to the magnetic towers.

We typically find that the launching region, which was defined in Paper I as the region where the velocity of the plasma changes from being perpendicular to the magnetic field to almost parallel to the magnetic field, is broader in dynamo simulations than in the non-dynamo simulations. Also, the disk surface, where the radial velocity changes sign by definition, is located at higher altitudes, although the thermal disk scale height is still about constant in time and about its initial value.

3.3. Outflow Launching: Accretion–Ejection

The magnetic field of the inner disk that is established in the simulations is similar to the usual structure favoring the magneto-centrifugal launching of the outflow. This type of jet formation has been previously found and discussed by many authors (Blandford & Payne 1982; Casse & Keppens 2004; Pudritz et al. 2007; Zanni et al. 2007; Murphy et al. 2010) as well as in our Paper I.

Therefore, in this section, we concentrate on the (outer) disk region where the magnetic field has evolved into a structure completely different from the previous simulations, namely, into a structure with the poloidal magnetic field being predominantly radial and a very strong toroidal component. In this part of the disk, it is the toroidal magnetic field that plays the key role in the launching (see Figure 4).

As the accretion–ejection process is governed by the magnetic torques, these torques need to be discussed in detail. The white line in Figure 4 marks the region where the magnetic torque changes sign. The torque is negative in the inner disk (inside the white line), where the angular momentum extraction from disk to outflow takes place, and positive in the disk corona, leading to the acceleration of the outflow material. In the region dominated by the magnetic loops at radii of $R \simeq 15$, we find that the torque is purely positive, thus playing a major role in the acceleration of the plasma. The blue line in Figure 4 separates two regions, where (1) the magnetic forces accelerate the matter in the direction of the outflow ($F_\theta > 0$, above the line), and (2) where the magnetic forces pinch the disk (below the line). In the disk area below this line, the main force lifting the matter into the outflow is the thermal pressure. The lines that mark the area where the pressure force is equal to the Lorentz force projected

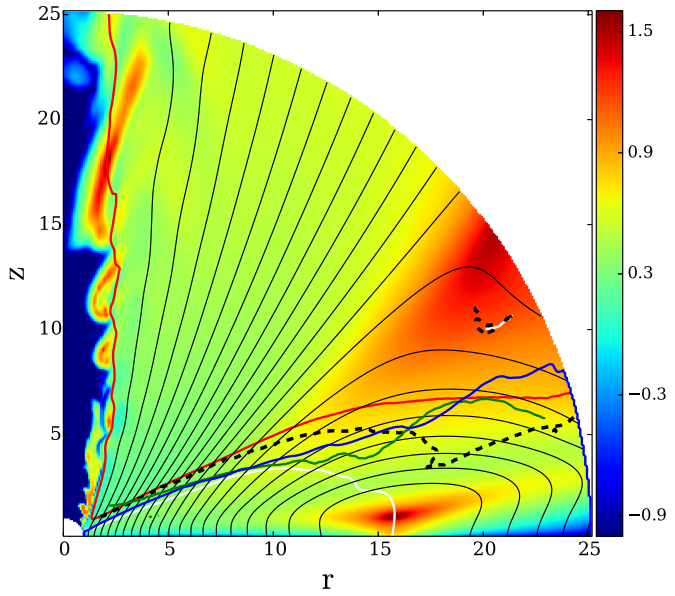

Figure 4. Distribution of the magnetic field components at $T = 1000$. Shown is the ratio of the toroidal to the poloidal magnetic field (colors, *logarithmic scale*); the poloidal magnetic field lines (thin black lines); the sonic surface (red line); and the locations where the Lorentz force components change sign, $F_\phi = 0$ (white line) and $F_\theta = 0$ (blue line). Further denoted are the locations where (1) the gas pressure force is equal to the Lorentz force, both projected parallel to the magnetic field (black dashed line), and (2) where the gas pressure force is equal to the Lorentz force both projected parallel to the velocity field (green line).

(A color version of this figure is available in the online journal.)

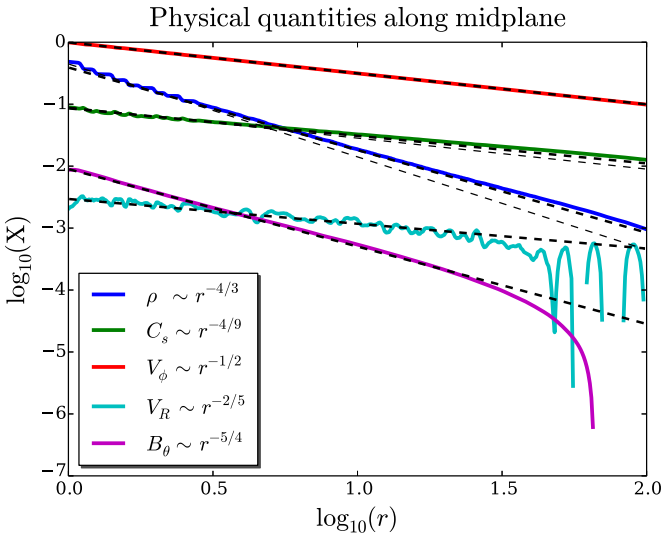

Figure 5. Physical quantities along the disk midplane for the reference dynamo simulation at $T = 10{,}000$. Colored lines correspond to different physical quantities, density ρ, sound speed C_s, rotational velocity V_ϕ, radial velocity V_R, and the magnetic field component B_θ. The thick dashed lines show the corresponding approximation by a power law. The thin dashed lines show the initial power-law distribution, slightly offset from the actual distribution at $T = 10{,}000$.

(A color version of this figure is available in the online journal.)

parallel to the magnetic field (black dashed line) and parallel to the velocity field (green line) are also shifted closer toward the disk midplane.

In the area above the loop-like structure, the toroidal magnetic field dominates the poloidal field. In this region, acceleration is mainly governed by the toroidal magnetic field pressure gradient.

It is worth noting that such a configuration does not reach steady state. This is already indicated by the misalignment between the magnetic field lines and velocity field. Furthermore, the blue lines in Figure 2 denote the launching area (see Paper I) where the velocity field changes from a direction perpendicular and parallel to magnetic field lines. The longer the simulation evolves, the larger the area that reaches steady state. In other words, the non-steady loop structure is moving outward along the disk.

3.4. Dynamical Profiles of a Dynamo-disk Driving Jets

Here we discuss the overall disk structure of the reference dynamo simulation. Figure 5 presents the radial profiles of a number of MHD variables measured at the disk midplane, and the power-law fits to them. The slight deviation between these lines shows how the disk structure changes after long time evolution. At time $T = 10{,}000$ we find distinct power laws for the profiles along the disk for radii up to $R \leqslant 40$. This is the radius that demarcates a steady state area from the rest of the disk, where the magnetic field is continuously generated. This is easiest to infer from the profile of the poloidal magnetic field profile, which starts deviating from the approximate power law at $R = 40$.

In order to better compare the analytical fits to the radial profiles resulting from the dynamo simulation to those without the dynamo (Paper I), we plotted the fits with the same power-law indices as for Paper I. We see that the actual profiles (for example, the density) show only a tiny deviation.

At time $T = 10{,}000$, we find the following numerical values for the power-law coefficients β_X for different variables at the midplane $X(r, \theta = \pi/2) \sim r^{\beta_X}$. The disk rotation remains Keplerian over the whole time evolution, therefore $\beta_{V_\phi} = -1/2$. The radial profiles for density and thermal pressure slightly change from their initial distributions. The power-law index of the density changes from $\beta_\rho = -3/2$ to about $\beta_\rho = -4/3$, while for the pressure it changes from $\beta_P = -5/2$ to about $\beta_P = -20/9$. We find $\beta_{V_R} = -2/5$ for the accretion velocity and $\beta_{B_\theta} = -5/4$ for the poloidal magnetic field. The accretion velocity remains subsonic everywhere in the disk with an accretion Mach number of $M_R \equiv V_R/C_s \simeq 0.08$. As expected, we find strong fluctuations in the area where the dynamo is active and field magnetic generation is ongoing.

Following Ferreira & Pelletier (1995) and considering the mass accretion rate $\dot{M}_{\rm acc} \sim R^2 \rho V_R$, it is easy to derive the ejection index $\xi = 2 + \beta_\rho + \beta_{V_R}$,[6] which is a measure of the efficiency of the outflow. We find $\xi = 0.25$, about the same value as for the non-dynamo simulation (see Paper I).

In this section, we have demonstrated that the radial profiles for disk dynamics along the midplane are very similar to the simulations including dynamo action and those without dynamo (in Paper I). We find several reasons for this explanation. First, in the case of a moderately weak magnetic field, the disk dynamics is primarily governed by the hydrodynamical quantities, but not so much the magnetic field. The power-law nature of the Keplerian rotation dominates the dynamics and forces the other hydrodynamical profiles into power-law distributions as well.

[6] Steady state and a power-law nature of the accretion rate is implicitly assumed.

Second, the magnetic field strength resulting from the disk evolution is of the same order for both approaches, $\mu \approx 0.01$, which can also lead to profiles with the same distribution.

3.5. Dynamo versus Non-dynamo Simulations

Here we discuss the major differences between the simulations with and without the mean-field $\alpha^2\Omega$ dynamo. As pointed out in the previous sections, the major difference between dynamo and non-dynamo simulations is the structure of the magnetic field and not so much the accretion disk hydrodynamics. The dynamo generates the magnetic field that is continuously spreading over the whole disk. In the early stage of the disk evolution, this makes a substantial difference. Later, when the inner part of the disk has reached steady state, this part of the disk looks very much the same except for a few details. One difference can be found concerning the disk wind close to the disk surface. In a dynamo simulation, the sonic surface and the Alfvén surface are located 20%–30% further up into the outflow. However, the magnetic lever arm (radius of the Alfvén point) is about the same. This is the result of the vertical component of the magnetic field being stronger with the lower inclination of the magnetic field with respect to the disk surface being more inclined toward the disk surface. The launching area, namely, the area where the velocity field changes from being almost perpendicular to the magnetic field into being parallel to the field (see Paper I), is now wider, while the disk surface stays at about the same level. Note that because of the evolving loop-like structure of the magnetic field, the field inclination with respect to the disk or the sonic surface does change in time and space, except the inner disk where steady state has established.

In order to study the jet properties with respect to the actual disk magnetization, we have performed several simulations, varying the μ_0 parameter in the definition of the diffusivity (Equation (5)). This parameter indirectly governs the resulting disk magnetization, as discussed above and also in Paper I. By running simulations with different μ_0, we were able to probe the resulting actual magnetization of the poloidal component in the inner disk over a range $\mu_{\rm act} = 0.01$–0.05. As shown in Paper I, it is in this range of magnetization where a change in the dominant launching mechanism takes place.

In comparison, we find that in our dynamo simulations that the disk and jet properties do not really differ for different actual magnetizations, and we cannot disentangle different launching mechanisms in the dynamo simulations. In contrast, the disk quantities as well as the jet integrals (see Paper I) behave rather similarly in this range of magnetization for both simulations.

In order to disentangle the causes for this similar evolution, we recall two points. The main reason why we can distinguish two different mechanisms in the non-dynamo simulation is the ability to generate a strong magnetic shear with a sufficiently weak poloidal magnetic field. This is possible because the diffusivity in the standard model depends only on the poloidal magnetic field. Thus, for a weak poloidal field, the diffusivity is also small, which helps sustain the strong magnetic shear. In contrast, in the current study, the magnetic diffusivity depends on the average *total* magnetic field in the disk. Therefore, a strong magnetic shear (a stronger toroidal magnetic field) directly increases the diffusivity, and, as a consequence, limits the magnetic shear.

This more subtle interrelation between the simulation parameters and physical processes again emphasizes the impact of the magnetic diffusivity model applied.

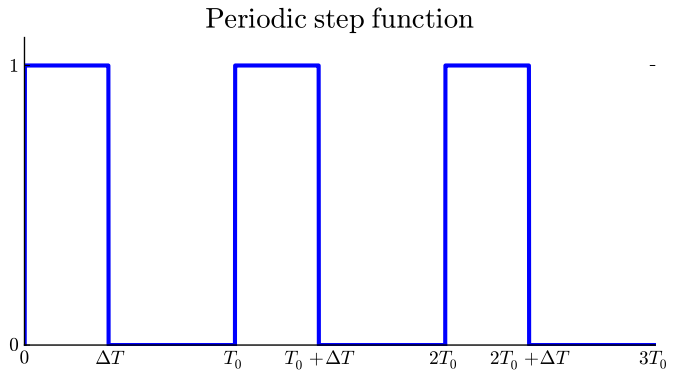

Figure 6. Periodic step function applied for the toy model of a time-variable disk dynamo. Here the dynamo α is simply modulated by the periodic step function. Thus, the dynamo is switched on after periods of nT_0 and switched off at $nT_0 + \Delta T$.

(A color version of this figure is available in the online journal.)

4. EPISODIC JET EJECTION TRIGGERED BY A TIME-VARIABLE DISK DYNAMO

In this section, we present simulation results of a toy model applying a time-dependent dynamo action. Our motivation is the following. The dynamo is intrinsically a stochastic phenomenon that in real accretion disks can be subject to strong fluctuations. Some accretion disks may exist in which the dynamo action is suppressed, while in other disks if certain conditions are met the dynamo can start to operate. Also, the dynamo quenching mechanism can stop an already working dynamo, and thus lead to a reconfiguration of the disk–jet system. Here we refer to the well-known solar cycle as an example. It is believed that a solar dynamo is responsible for the reconfiguration of the magnetic field of the Sun. The strong toroidal field component reveals itself as sunspots with a cyclic appearance. This solar periodicity can be understood as triggered by a constantly operating dynamo (or maybe by different types of dynamos). Another interesting feature of the solar activity in this respect is that it exhibits long-term minima (Eddy 1976), during which there were no sunspots observed at all. It is believed that during these minima the dynamo action is either strongly suppressed or completely switched off.

For our accretion–ejection simulations we follow a preliminary approach and apply a simple toy model to explore the impact of such an effect for jet-launching. We multiply the spatial α profile with a time-dependent function. Here we apply a periodic step function (Figure 6) by which we continuously switch on and off the dynamo in the disk. The periodic step function is characterized by its period T_0 and time length of a step function ΔT. In other words, T_0 is the period of the dynamo cycle and ΔT the activity cycle of the dynamo. Below, we present the simulation with $T_0 = 1000$ and $\Delta T = 400$.

Essentially, the modulation of the dynamo-α leads to the variation of the disk magnetization (Figure 7) with the same periodicity. The strength of diffusivity is chosen such that without a dynamo working in the disk, the advection of the magnetic flux with the accreted material cannot balance the outward diffusion of the magnetic field. This eventually results in a decrease of the disk magnetization. As previously shown (see Paper I for details), there exists a limit on the strength of the magnetization below which the disk cannot sustain a jet. When the disk magnetization decays below the level of $\mu \approx 10^{-3}$ the

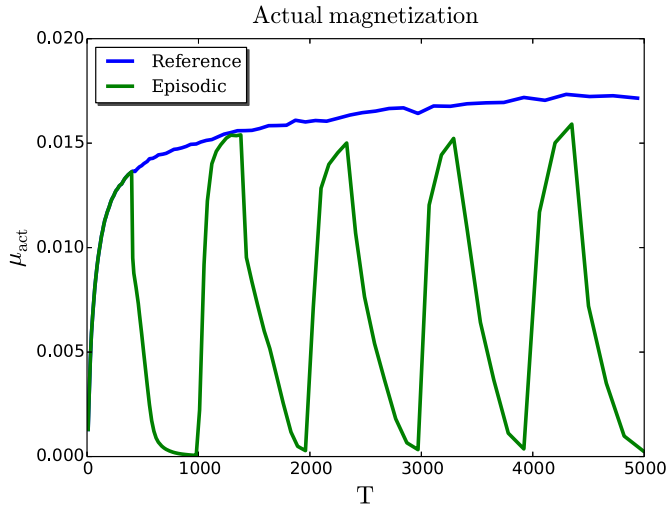

Figure 7. Time evolution of the actual disk magnetization μ_{act} of the reference dynamo simulation (blue line) and time-dependent dynamo simulation (green line).

(A color version of this figure is available in the online journal.)

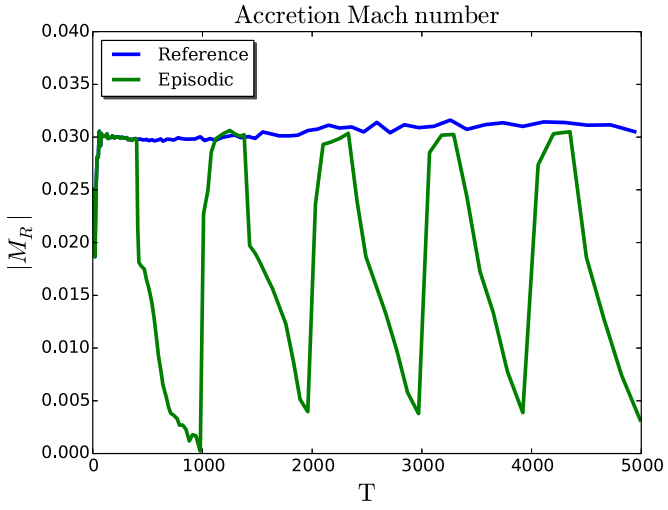

Figure 8. Time evolution of the accretion Mach number M_R of the reference dynamo simulation (blue line) and time-dependent dynamo simulation (green line).

(A color version of this figure is available in the online journal.)

strong jet disappears. On the other hand, if the dynamo action is re-established, the disk magnetization grows again and the outflow is re-launched.

We performed a series of parameter runs, varying both T_0 and ΔT. In principle, different scenarios are possible, depending not only on the period of the step function, but also on the magnetic diffusivity and the dynamo parameter (and various combinations of those).

In order to generate episodic ejection events, and thus re-establish a jet-driving magnetic field structure, several conditions have to be met by the dynamo process. First, the dynamo must be strong enough in order to generate the magnetic field sufficiently fast. Second, in order to suppress the jet ejection during consecutive switch-off periods, $(nT_0 - \Delta T)$, these periods should be sufficiently long and/or the magnetic diffusivity should be sufficiently high. Only when the inner disk magnetization decreases below $\mu \approx 10^{-3}$, the jet launching can no longer be sustained and the strong outflow disappears. The overall evolution of these processes depends on both the periods T_0 and ΔT of the step function.

The interplay among dynamo action, accretion, and diffusion may lead to different scenarios for the episodic ejection events. If the switch-off period of the dynamo is shorter than the timescale for the magnetic field to diffuse out, the jet ejection will be constantly sustained, and the jet mass and energy fluxes will be just modulated. If the disk magnetization decays below the value than is necessary to drive a jet, and if the dynamo is weak or works only for a short time, the magnetic field will not be re-established adequately, and, therefore no new jet will be ejected.

Applying such a toy model we are able to produce *episodic jet events*, during which the jet as well as the disk variables undergo substantial changes. The change of the disk magnetization directly affects both accretion and ejection processes. As the magnetization varies in time, the other physical quantities also vary. As discussed in Paper I, the accretion Mach number $M_R = V_R/C_s$ is tightly related to the disk magnetization. Figure 8 clearly shows that variations in the disk magnetization triggered by the time-dependent dynamo directly affect the disk accretion.

Figure 9 shows the time evolution of a time-dependent dynamo simulation. As for the case when we discuss the evolution of the reference simulation (Figure 1), we show only a small cylindrical part of the whole spherical domain. We kept all parameters the same as in the reference dynamo simulation, just folding the dynamo term with the periodic step function. Obviously, compared to the reference dynamo simulation, the overall structure of the disk–jet system changes in time—substantially, and not smoothly as for the case of a constant dynamo effect. The dynamo is working until $T = 400$ when it is switched off. Therefore, before $T = 400$ the evolution of the disk and outflow was identical to that previously discussed (see Figure 1). Between $T = 400$ and $T = 1000$ the generation of the magnetic field by the dynamo was switched off. As a consequence, the magnetic field diffuses substantially and the jet velocity decreases. Although the disk magnetization is continuously decreasing, a weak outflow is still present. It is the period when the dynamo is switched off $(T_0 - \Delta T)$ which indirectly limits the disk magnetization. The more time is given to diffuse away the magnetic field, the smaller the resulting disk magnetization will be in the period when the dynamo is switched off.

At $T = 1000$, the dynamo is switched on again, and the generation of the magnetic field is re-established. Because the dynamo-α is rather high and a substantial magnetic flux has remained from the previous cycle, it takes rather little time to reach sufficient magnetization again for strong outflow launching. Once the substantial magnetization of the disk is reached, $\mu \approx 10^{-3}$, the outflow is re-launched. from the inner part of the disk, the outflow re-establishes in the outward direction. Advection of the magnetic flux, together with the accretion material, leads to amplification of the magnetization. At $T = 1400$ the typical magneto-centrifugal structure of the magnetic field is re-established and a quasi-steady outflow re-appears, thus closing the activity cycle. Essentially, these magnetic cycles and subsequent jet ejection are repetitive. However, they are not necessarily identical, due to the magnetic field structure remaining from the previous cycle.

We note that the dynamo mechanism discussed above is able to regenerate the magnetic field in the disk completely.

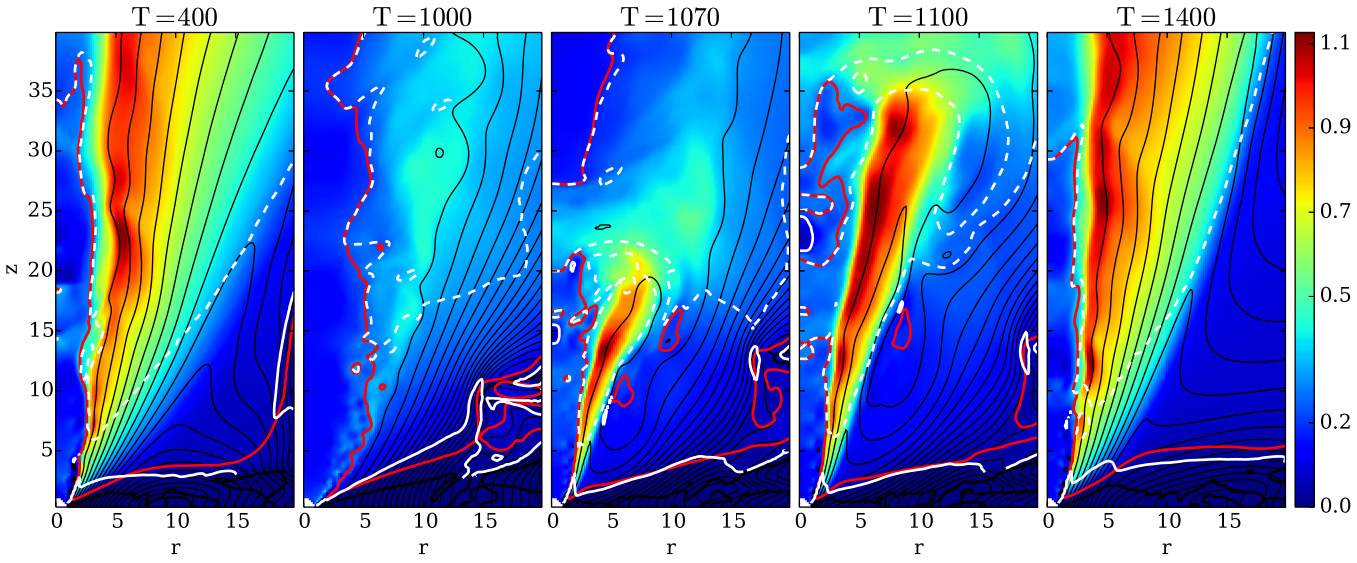

Figure 9. Time evolution of the disk–jet structure of the simulation with time-dependent dynamo action. Only a small cylindrical part of the whole spherical domain is presented. Shown is the velocity (colors), the poloidal magnetic field lines (thin black lines), and the sonic (red line), the Alfvén (white line), and the fast magnetosonic (white dashed line) surfaces.

(A color version of this figure is available in the online journal.)

This is indeed different from the case of simple modulation by the change in the magnetic diffusivity parameter $\alpha_{\rm ssm}$. In Paper I, we have shown that the diffusivity parameter $\alpha_{\rm ssm}$ is very crucial for determining the *actual* disk magnetization. Without a disk dynamo, we were able to modulate the outflow simply by varying the $\alpha_{\rm ssm}$ parameter; however, it was impossible to drastically affect the structure of the magnetic field, as we can now do with the dynamo.

4.1. Structure and Evolution of the Episodic Jets

Figure 10 presents a time series of snapshots of the high-speed outflow propagating close to the axis. Again, we show only a small cylindrical part of the whole spherical domain, choosing time and space scales in order to display the main outflow features. In order to show the typical stages of the episodic ejection generation and propagation we have chosen the three dynamical time step times $T = 450, 1450, 3450$ of our simulation lasting 10,000 dynamical time steps.

First, we see how the outflow is initially generated (thus from the first cycle of dynamo activity) and then propagates throughout the hydrostatic corona. After switching off the dynamo at $T = 400$, the jet weakens until it almost completely disappears. The dynamo becomes active again at $T = 1000$. At $T = 1450$ that first ejection has already reached $R \approx 1100$, just when another "jet" has been launched. At an even later time, $T = 3450$, this second knot has established an outflow, and a third knot is launched.

The timescales we have chosen are such that we can follow multiple ejection events on our grid. The time $T = 1000$ would correspond to about $T/2\pi$ inner disk rotations, thus about a year if we apply the inner disk radius $R_0 = 0.1$ AU. For comparison, jet observations of young stars suggest the timescales between the knots $\tau_{\rm knot} \simeq \Delta L/v_{\rm jet} \sim$ to be about 10 yr. If the knot generation mechanism is indeed triggered by a disk dynamo, the timescale for the field reversals must be longer.

In the two middle panels of Figure 10, we clearly see two fast rapidly moving gas ejections. These parcels of ejected material are separated from each other by the typical period of the dynamo T_0, corresponding to about $1000r_0$ distance between them. The ejected material rams into the gas which is left from the previous parcel and which moves with lower velocity. Shocks that can be clearly seen in the density map[7] are generated. We may interpret the repeated ejections as jets knots; however, a more detailed (future) investigation would be necessary to confirm this picture.

We may clearly identify the signatures of the inflow from the inner coronal boundary into the domain along the outflow axis for low $z < 200$. As discussed above, this axial inflow is essential to provide the gas pressure that balances the collimation forces of the outflow in the vicinity of the disk. In our simulations, it is injected artificially by the boundary condition; however, an astrophysical interpretation could be that of a wind driven by the central object.

4.2. Self-induced Magnetic Field Regeneration

As discussed in the beginning of this section, the dynamo action is a stochastic, highly non-linear process. We can expect that under certain conditions the non-linear evolution of the dynamo is more pronounced than under other conditions. In this section, we show preliminary results of simulations evolving in a more stochastic way and which may be considered as a more natural "switch" for the dynamo mechanism. No artificial on/off switch has been applied. These simulations consider a self-induced regeneration of the magnetic field without applying any additional constraints such as a periodic step function in the time-dependent dynamo profile.

In our simulations we have observed very similar self-induced regeneration processes of the magnetic field under different conditions. Thus, there seem to be several ways how a self-induced switch of the dynamo regeneration can take place. Some of them require the presence of a quenching mechanism. Without that, the magnetic flux will be continuously generated in the inner disk and will eventually fill the entire disk with magnetic field of one dominant polarity.

[7] The shock structure is also visible in the pressure distribution and also in the jumps in the velocity profile along the jet (not shown as figure).

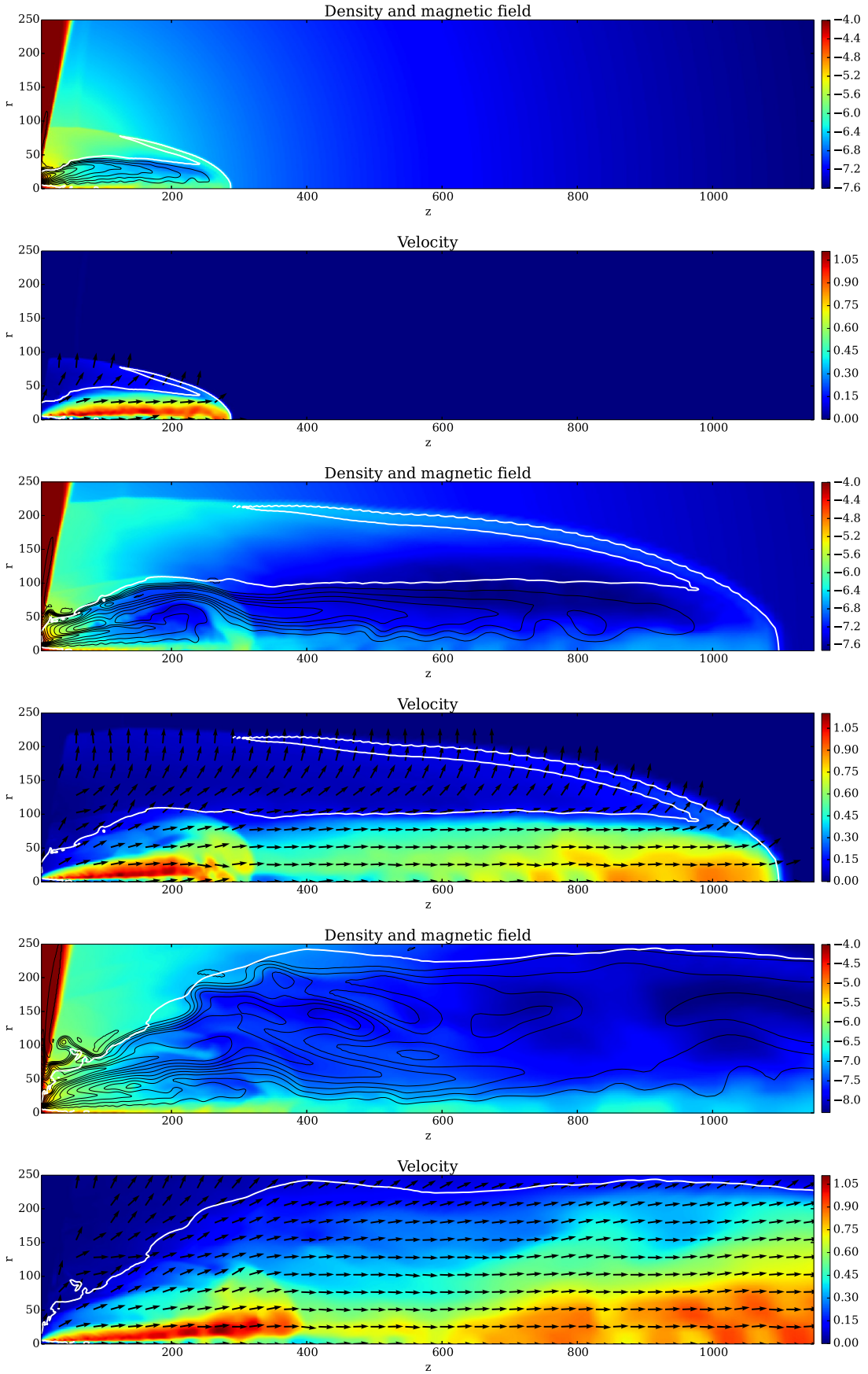

Figure 10. Structure of the simulation with time-dependent dynamo action shown at $T = (450, 1450, 3450)$, from top to bottom. Plots are grouped in twos. Shown by color density logarithm (upper plot) and jet speed (lower plot). Maximum density is set to 10^{-4}. Black lines show the magnetic field. The white line represents the sonic surface. Arrows show the normalized velocity vectors.

(A color version of this figure is available in the online journal.)

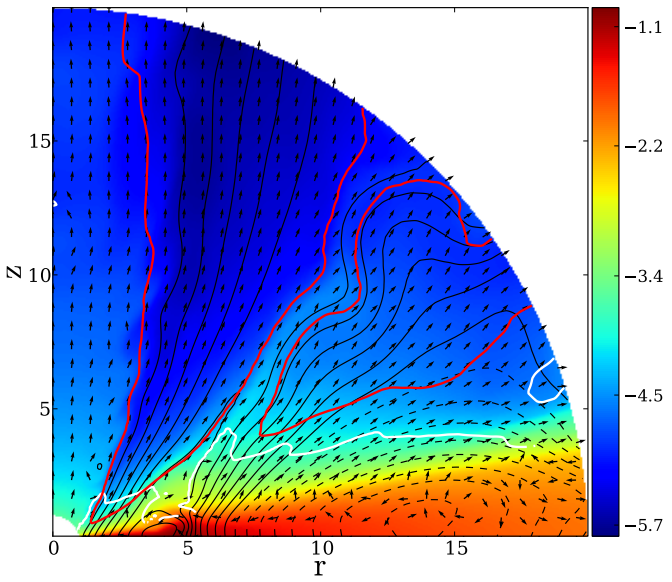

Figure 11. Example simulation resulting in two opposite magnetic loops generated by the dynamo. Shown is the mass density (colors, logarithmic scale), the poloidal magnetic field lines (black lines, dashed lines show opposite magnetic flux), the sonic surface (red line), and the Alfvén surface (white line) at time $T = 1000$. Arrows show normalized velocity vectors.

(A color version of this figure is available in the online journal.)

One possibility to establish a self-induced switch for the magnetic field, is to initiate the simulation with the disk filled by toroidal magnetic field of a different polarity. Then the poloidal magnetic field that is generated by the dynamo will have different polarities as well. Constant field amplification will lead to the accretion/advection of this magnetic structure. As these structures move toward the center, the generation of the magnetic field in the innermost structure will be quenched, while the magnetic flux in the outer disk will continue to grow. As a consequence these structures merge (by diffusion) and decay, and a quiescent period of outflow launching follows.

Another way is to link the dynamo term to the toroidal magnetic field. As discussed above, the poloidal magnetic field in the outer disk has the opposite polarity to the inner disk magnetic field. Thus, in this case an additional feedback channel is provided that, under certain circumstances, can lead to a more fluctuating evolution of the disk–outflow system. The last example that surprisingly showed such self-induced regeneration of the magnetic field is our reference simulation, but with lower dynamo-term $\alpha_{\rm D} = -0.03$. Figure 11 shows the magnetic field structure in the disk of one such simulation. We have observed that sometimes the dynamo generates several magnetic field loops in the disk. While the magnetic field in the inner disk is able to quench the dynamo, in the outer disk the magnetic field is continuously amplified. The magnetic flux generated in the outer disk is of opposite polarity. If advected inward, it will eventually reconnect with the magnetic flux in the inner disk. During this cancellation (reconnection) process, the disk magnetization in the jet launching region will decrease below a critical level, jet launching will decay, and the outflow will disappear. At later stages, when the magnetic field remaining from the reconnection process becomes sufficiently amplified by the dynamo, the outflow will be launched again.

The details of the process of magnetic field regeneration in fact depends on many model parameters, in particular the magnetic diffusivity model. Although this might be an interesting mechanism triggering episodic events, we do not present details here, since we were not yet able to get it to work robustly and to run the simulation longer than for just a few regenerations.

5. CONCLUSIONS

We have presented results of MHD simulations investigating the generation of the magnetic field by the accretion disk dynamo in the context of jet and outflow launching. The time evolution of the disk structure is self-consistently taken into account. The simulations are performed treating all three field components while preserving/keeping axial symmetry. We apply the MHD code PLUTO-4.0, which we have modified for the mean-field $\alpha^2\Omega$ dynamo problem in the induction equation.

In the present work, we explored the generation of a large-scale global magnetic field. Our simulations were initiated by the purely radial magnetic field with magnetization $\mu_{\rm init} = 10^{-5}$. We showed in detail how the magnetic field is being generated and through which consecutive stages it evolves, acquiring in the end the ability to launch jets and outflows. In this respect, our simulations can be seen as a continuation of the early works by von Rekowski et al. 2003 and von Rekowski & Brandenburg 2004. In our paper, we concentrated more on the jet and outflow generation and propagation.

One advantage of our simulations is that our model keeps the disk magnetization at a rather low level. Therefore, the magnetic field does not substantially affect the disk hydrodynamics, and allows us to evolve our simulations for very long time. Each simulation has been evolved at least up to $T = 10{,}000$ on a spherical domain with $R = [1, 1500]$.

In the following, we summarize our main results.

1. In our simulations treating a mean-field disk dynamo, we distinguish two main features in the magnetic field structures. The magnetic field of the inner disk that is similar to the commonly found open field structure, favoring a magneto-centrifugal launching of the outflow. The poloidal magnetic field of the outer part of the disk is highly inclined and predominantly radial. Differential rotation induces a very strong toroidal component from it. Such a structure is similar to what is known as a tower jet or Poynting jet in literature. In this part of the disk, it is the toroidal magnetic field that plays a key role in outflow launching. First, below the disk surface ($V_R = 0$) the matter is lifted by the buoyant force of the magnetic field, and thus, by the gradient of the thermal pressure. Starting from the disk surface ($V_R = 0$), the matter is further accelerated by the pressure gradient of the toroidal magnetic field. The outflows from the outer part of the disk are typically slower, denser, and less collimated, thus corresponding to a higher mass loading.
2. In principle, the dynamo can fill the entire accretion disk with magnetic flux. Thus, if the dynamo action is not quenched, magnetic flux is continuously generated, diffuses outward along the disk until it fills the entire disk. This loop-like structure of the magnetic field, which is typical for a dynamo, propagates further outward.
3. As soon as the disk magnetization reaches a critical limit, $\mu > 10^{-3}$, disk winds are launched and can be accelerated to super-magnetosonic speed. This result is complementary to our earlier simulations that do not consider dynamo (Stepanovs & Fendt 2014b), and where the critical magnetization was obtained just from advection of magnetic flux by accretion. Thus, again we can confirm the longstanding

belief that disk magnetization plays a key role in outflow launching. In the inner disk, the rate of generation of magnetic field by the dynamo is higher, leading to a strong gradient of the disk magnetization.

4. We have further invented a toy model triggering a time-dependent efficiency of the mean-field dynamo. In that model approach, we periodically switch the dynamo on and off. This strongly affects the magnetic field structure. The decay of magnetic flux by diffusion can be completely balanced by the dynamo that regenerates the magnetic field. As a consequence, the duty cycles of the dynamo action can lead to episodic jet ejection, depending on the disk magnetization obtained during dynamo activity. When the dynamo is suppressed and the disk magnetization falls below a critical value, $\mu \approx 10^{-3}$, the generation of outflows as well as the accretion is substantially inhibited. We have chosen the timescale of the dynamo cycle and the corresponding timescale for the episodic ejections to be somewhat shorter compared to the observed values, just because we wanted to follow several events in the same simulation box. However, the main—and general—result is that we can steer the episodic ejection and *large-scale jet knots* by the *disk-intrinsic dynamo*, which is time-dependent and regenerates the jet-launching magnetic field.
5. Concerning the disk hydrodynamics, we find that the accretion velocity follows the same power law $\beta_{V_R} \approx -2/5$ for the simulations with and without dynamo. This is interesting also because we have applied slightly different diffusivity models, leading to different magnetic field structures. Nevertheless, the accretion profiles are approximately the same. As a consequence, we also find approximately the same ejection index $\xi \approx 0.25$.
6. Although the dynamo and non-dynamo simulations are significantly different, the launching mechanism of the fast jet is primarily the same. Thus, from a purely observational point of view, one would not yet be able to distinguish whether the jets are launched from a dynamo-generated magnetic field or from a magnetic field advected from the interstellar medium.

In summary, we have shown the accretion–ejection evolution considering a magnetic field self-generated by a mean-field disk dynamo. Repetitive ejection could be obtained by a time-dependent dynamo α. A future step could be to consider the dynamo action for the strong-field case. That might be realized by implementing both an MRI dynamo and a Parker dynamo by means of different dynamo α. Another step would be to have a more direct link between the actual magnetic field and the dynamo.

We thank Andrea Mignone and the PLUTO team for the opportunity to use their code. The simulations were performed on the THEO cluster of the Max Planck Institute for Astronomy. This work was partly financed by the SFB 881 of the German science foundation DFG.

APPENDIX

RESOLUTION STUDY

We shortly discuss the results of our resolution study. We have performed simulations with a grid resolution of 0.75, and 1.5 times our standard resolution of $N_\theta = 128$ cells per quadrant, corresponding to $N_\theta = 96$ and $N_\theta = 192$ cells per quadrant, or approximately 12 or 24 cells per disk height 2ϵ compared to 16 cells per disk height in our reference run.[8]

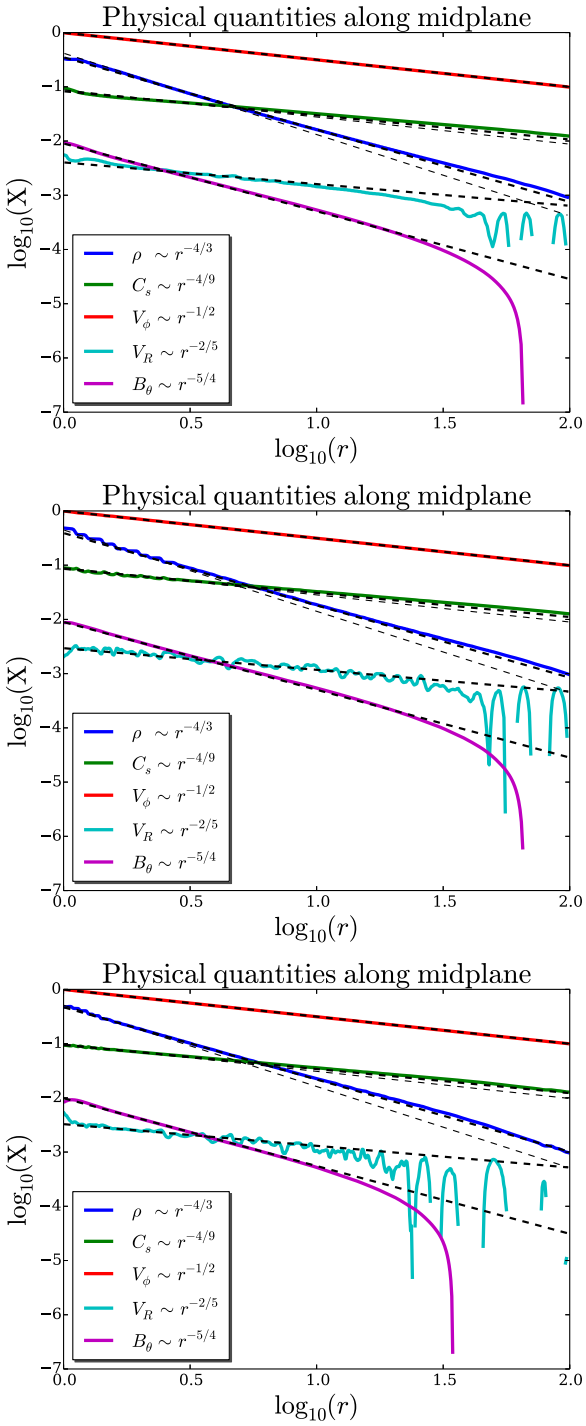

Figure 12. Resolution study. Physical quantities along the midplane for the simulations with different resolution at $T = 10{,}000$. From top to bottom the resolution is (12, 16, 24) cells per disk height (2ϵ). Colors show different variable profile, thick dashed lines correspond to certain power laws, and the mismatched thin dashed lines correspond to initial distributions of variables.

(A color version of this figure is available in the online journal.)

Figure 12 shows the dynamical profiles the three simulations of our resolution study. The radial profiles are plotted along the

[8] Note that once the resolution in the θ direction and the radial extent of the disk is chosen, the resolution in the R direction is uniquely determined (see Section 2, or Paper I).

midplane for various dynamical variables at time $T = 10{,}000$. As discussed in Section 3.4 these profiles can be nicely fitted by power laws. The same power-law index also provides the same ejection to accretion index. Therefore, we conclude that our results are not resolution dependent.

However, several differences between these curves can be noticed. The inner part of the disk for the simulation with lower resolution indicates a substantial deviation from the corresponding power law. We also find that for a lower resolution the accretion speed increases, and, as a consequence, the overall density in the disk decreases. This highlights the effect of the numerical viscosity that enhances the angular momentum transfer in the disk. On the other hand, the magnetic field is diffused out faster and to a larger distance. This indicates a higher numerical resistivity for the case of lower resolution.

REFERENCES

Arlt, R., & Rüdiger, G. 2001, A&A, 374, 1035
Armitage, P. J., Livio, M., & Pringle, J. E. 1996, ApJ, 457, 332
Bardou, A., von Rekowski, B., Dobler, W., Brandenburg, A., & Shukurov, A. 2001, A&A, 370, 635
Blandford, R. D., & Payne, D. G. 1982, MNRAS, 199, 883
Brandenburg, A., & Campbell, C. 1997, in Accretion Disks: New Aspects, ed. E. Meyer-Hofmeister & H. Spruit (Lecture Notes in Physics, Vol. 487; Berlin: Springer), 109
Brandenburg, A., & Donner, K. J. 1997, MNRAS, 288, L29
Brandenburg, A., Nordlund, A., Stein, R. F., & Torkelsson, U. 1995, ApJ, 446, 741
Brandenburg, A., Sokoloff, D., & Subramanian, K. 2012, SSRv, 169, 123
Brandenburg, A., & Subramanian, K. 2005, PhR, 417, 1
Brandenburg, A., & von Rekowski, B. 2007, MMSAI, 78, 374
Casse, F., & Keppens, R. 2002, ApJ, 581, 988
Casse, F., & Keppens, R. 2004, ApJ, 601, 90
Eddy, J. A. 1976, Sci, 192, 1189
Fendt, C. 2006, ApJ, 651, 272
Fendt, C. 2009, ApJ, 692, 346
Fendt, C., & Čemeljić, M. 2002, A&A, 395, 1045
Fendt, C., & Elstner, D. 1999, A&A, 349, L61
Fendt, C., & Elstner, D. 2000, A&A, 363, 208
Fendt, C., & Sheikhnezami, S. 2013, ApJ, 774, 12
Ferreira, J. 1997, A&A, 319, 340
Ferreira, J., & Pelletier, G. 1995, A&A, 295, 807
Fromang, S. 2013, in EAS Publications Series, Vol. 62, Role and Mechanisms of Angular Momentum Transport During the Formation and Early Evolution of Stars, ed. P. Hennebelle & C. Charbonnel (Cambridge: Cambridge Univ. Press), 95
Gammie, C. F., & Menou, K. 1998, ApJL, 492, L75
Hayashi, M. R., Shibata, K., & Matsumoto, R. 1996, ApJL, 468, L37
Johansen, A., & Levin, Y. 2008, A&A, 490, 501
Kato, Y., Hayashi, M. R., & Matsumoto, R. 2004, ApJ, 600, 338
Krasnopolsky, R., Li, Z., & Blandford, R. 1999, ApJ, 526, 631
Krause, F., & Rädler, K.-H. 1980, Mean-field Magnetohydrodynamics and Dynamo Theory (Oxford: Pergamon Press)
Lovelace, R. V. E., Romanova, M. M., & Bisnovatyi-Kogan, G. S. 1995, MNRAS, 275, 244
Lynden-Bell, D. 1996, MNRAS, 279, 389
Lynden-Bell, D., & Boily, C. 1994, MNRAS, 267, 146
Meliani, Z., Casse, F., & Sauty, C. 2006, A&A, 460, 1
Mignone, A., Bodo, G., Massaglia, S., et al. 2007, ApJS, 170, 228
Murphy, G. C., Ferreira, J., & Zanni, C. 2010, A&A, 512, A82
Ouyed, R., & Pudritz, R. E. 1997, ApJ, 482, 712
Pelletier, G., & Pudritz, R. E. 1992, ApJ, 394, 117
Porth, O., & Fendt, C. 2010, ApJ, 709, 1100
Pudritz, R. E. 1981a, MNRAS, 195, 897
Pudritz, R. E. 1981b, MNRAS, 195, 881
Pudritz, R. E., Ouyed, R., Fendt, C., & Brandenburg, A. 2007, in Protostars & Planets V, ed. B. Reipurth, D. Jewitt, & K. Keil (Tucson: Univ. Arizona Press), 277
Pudritz, R. E., Rogers, C. S., & Ouyed, R. 2006, MNRAS, 365, 1131
Rekowski, M. v., Rüdiger, G., & Elstner, D. 2000, A&A, 353, 813
Rozyczka, M., Joung Turner, N., & Bodenheimer, P. 1995, MNRAS, 276, 1179
Sheikhnezami, S., Fendt, C., Porth, O., Vaidya, B., & Ghanbari, J. 2012, ApJ, 757, 65
Shibata, K., & Uchida, Y. 1985, PASJ, 37, 31
Stepanovs, D., & Fendt, C. 2014, ApJ, 793, 31 (Paper I)
Tout, C. A., & Pringle, J. E. 1992, MNRAS, 259, 604
Tzeferacos, P., Ferrari, A., Mignone, A., et al. 2009, MNRAS, 400, 820
Ustyugova, G. V., Koldoba, A. V., Romanova, M. M., Chechetkin, V. M., & Lovelace, R. V. E. 1995, ApJL, 439, L39
Ustyugova, G. V., Lovelace, R. V. E., Romanova, M. M., Li, H., & Colgate, S. A. 2000, ApJL, 541, L21
Vaidya, B., Fendt, C., & Beuther, H. 2009, ApJ, 702, 567
von Rekowski, B., & Brandenburg, A. 2004, A&A, 420, 17
von Rekowski, B., Brandenburg, A., Dobler, W., Dobler, W., & Shukurov, A. 2003, A&A, 398, 825
Zanni, C., Ferrari, A., Rosner, R., Bodo, G., & Massaglia, S. 2007, A&A, 469, 811